RSC Advances

ROYAL SOCIETY OF CHEMISTRY

www.rsc.org/advances

RSC Advance

ARTICLE

Effect of surface oxygen/nitrogen groups on hydrogen chloride removal using modified viscose-based activated carbon fibers

Received 00th January 20xx,
Accepted 00th January 20xx

DOI: 10.1039/x0xx00000x
www.rsc.org/

Zean Wang[a], Hao Liu[a], Kang Zhou[a], Peifang Fu[a], Hancai Zeng[a], Jianrong Qiu[a]

Activated carbon fibers (ACFs) can effectively remove pollutants including nitrogen oxides, sulfur oxides and trace metals due to their rich micropores and large specific surface area. This work aims to investigate the roles of surface oxygen and O-containing nitrogen species on the removal of hydrogen chloride (HCl) using viscose-based ACFs. To evaluate the effect of surface oxygen and O-containing nitrogen groups, commercial viscose-based ACFs were treated by thermal treatment (900 °C) and chemical impregnations using H_2O_2, HNO_3 and Cu $(NO_3)_2$. Pore volumes, average pore size and specific surface area were separately characterized by t-plot method, density functional theory and Brunauer-Emmett-Teller theory. Surface morphology of the ACFs was observed by scanning electron microscope. X-ray photoelectron spectroscopy (XPS) technique was applied to determine specific ratios of surface oxygen and nitrogen groups. Temperature programmed desorption was performed to investigate HCl adsorption behaviors over the ACFs. As experimental results, thermal process decreased the oxygen groups while H_2O_2 impregnation increased the oxygen groups (especially the carbonyl and carboxyl). Nitroso and nitro groups were introduced onto the carbon surface after HNO_3 and Cu $(NO_3)_2$ treatments. The removal efficiency of HCl was improved slightly by H_2O_2 modification due to the increase of oxygen groups, significantly by HNO_3 and Cu $(NO_3)_2$ treatments because of newly formed O-containing nitrogen groups. Nitroso and nitro groups show significant promotion on HCl retention ability over the ACFs surface. Moreover, HCl removal efficiency was much more influenced by nitroso than nitro groups.

Introduction

Air has been severely polluted by various industrial emissions, such as sulfur oxides (SO_X), nitrogen oxides (NO_X), elemental mercury (Hg^0), volatile organic compounds (VOC) and some chlorinated pollutants[1]. Gaseous hydrogen chloride (HCl), main component of chlorinated contaminants, can greatly threaten human life even with very small amount in air[2]. In recent years, hazardous air pollutant emissions have been regulated by increasingly stringent government legislation in China.

For the past decade, activated carbon fibres (ACFs) have been widely used in air purification on the removal of contaminants such as SO_X, NO_X, VOC and Hg^0 due to their low cost, large specific surface area, highly porous structure and various surface functional groups[3-14]. It is recognized that the textural properties and surface chemistry are the most important properties of ACFs for applications in adsorption and catalytic processes. Bansal and Suzuki reported that the adsorption capacity of ACFs was closely related to the textural properties as well as surface chemistry, in particular the amount of surface functional groups[6, 15]. Unfortunately, untreated ACFs only have very small amount of surface functional groups, and hence various treatments, i.e. acid and alkaline modifications, have been adopted to modify the carbon surface [16, 17]. Park used oxygen plasma to yield oxygen enriched ACFs to capture HCl gas[18]. After several times of treatment, the HCl adsorption capacity of ACFs can be improved as much as 300 % due to the increase of surface oxygen groups, however, the high cost limits the practical applications. Meanwhile, more cost-effective ammonia modification was applied by Mangun to obtain ACFs of high HCl adsorption efficiency[19]. Ammonia treatment significantly enhanced HCl adsorption due to the introduction of H-containing nitrogen groups, i.e. =NH, $-NH_2$, $-NH_3$, CN, etc. However, O-containing nitrogen species, i.e. nitroso ($-NO_2$) and nitro ($-NO_3$) groups, deserve much attention since those nitrogen species are generally associated with the catalytic removal of acidic gases, i.e SO_2[20] and NO[21], whereas few relevant work was conducted. Particularly, among the studies regarding HCl capture, ACFs were mostly treated by just one single method which is not sufficient enough to fully understand the influence of surface groups, because single method could not only affect the surface chemistry but also the textural properties of carbon materials.

In this paper, both physical and chemical techniques, i.e. thermal treatment and chemical impregnations in H_2O_2, HNO_3 and $Cu(NO_3)_2$ solution, were employed to modify the ACFs surface, and scanning electron microscopy (SEM) was utilized to observe the morphology changes. Moreover, the amounts of surface oxygen and nitrogen groups were thoroughly examined through X-ray photoelectron spectra (XPS), and atom ratios of O/C and N/C were given based on elemental analysis results. Subsequently, HCl adsorption was carried out and temperature programmed desorption (TPD) was used to investigate HCl adsorption behavior over the ACFs surface. Based on such information, effects of surface oxygen and/or

[a]State Key Laboratory of Coal Combustion, Huazhong University of Science and Technology, Wuhan 430074, China

nitrogen groups on the removal efficiency of HCl were comprehensively discussed.

Materials and methods

Materials preparation

The initial material was commercial viscose-based ACFs cloth, manufactured by Jiangsu Sutong Carbon Fiber Co. Ltd. (China). To remove possible impurities, ACFs cloth was cut into pieces (5 × 5 × 3 mm) and washed with deionized water until the pH is neutral, then was dried in flowing air at 105 °C for 24 h. This material was labelled ACF-AR for comparison. Oxygen-poor ACFs were prepared through thermal treatment, denoted as ACF-1: ACFs cloth was heated in a tube furnace at 900 °C for 1 h at 10 °C/min to decrease surface oxygen groups, then was cooled to room temperature under argon protection. Oxygen-rich sample ACF-2 was obtained as following: ACFs cloth was soaked in H_2O_2 solution (30 wt. %), then stirred at room temperature for over 24 h, and finally washed with deionized water until the filtrate was neutral. The nitrogen-rich sample ACF-3 was obtained with the similar process as ACF-2 using diluted nitric acid solution (30 wt. %) as impregnate. Meantime, acidic $Cu(NO_3)_2$ solution (8 wt. %) without strong oxidation was employed to treat the ACFs cloth as comparison, and the treated sample was denoted as ACF-4. These prepared ACFs were dried in an electric oven under flowing argon for at least 6 h (60 °C for 3 h and 80 °C for 3 h) and stored in a sealed vial for further utilization.

Pore and morphology characterizations

Before measurements ACFs were degassed to 5×10^{-7} Pa for 12 h at 110 °C. The specific surface area was calculated according to the N_2 adsorption isotherms at 77 K (ASAP2020, Micrometrics, U.S.) using the Barrett-Emmett-Teller (BET) equation. First, pore volumes were estimated from nitrogen adsorption and desorption isotherms data obtained at 77 K under the relative pressure (P/P_o) of 10^{-6}~1 [22]. Then t-plot method was applied to determine the micropore volume [23, 24]. Afterwards, the average pore size was calculated according to density functional theory [25]. The SEM images were performed on a scanning electron microscope (Quanta 200, N.L.).

Elemental analysis

An elemental analyzer (EL-2, Elementar, D.E.) was used to characterize the amounts of carbon, hydrogen, nitrogen and sulfur in the ACFs sample. Oxygen was determined by mass difference assuming the ACFs consisted only of carbon, hydrogen, nitrogen, sulfur and oxygen.

X-ray photoelectron spectra

XPS patterns were collected by an X-ray photoelectron spectrometer (XSAM800, Kratos Analytical Ltd, U.K.) using Mg Kα (1253.6 eV) radiation. The survey spectra were obtained between 0 and 1000 eV with an energy step of 0.25 eV and recorded in the fixed analyzer transmission mode (pass energy = 40eV). During analysis the pressure in the sample analysis chamber was held below 1×10^{-9} Torr. Then the spectra were calibrated by C1s (284.6 eV), N1s (400 eV) and Cl2p (201.1 eV) before determining the distribution of surface functional groups. After a Shirley-type background subtraction the spectra of C1s and N1s were fitted by asymmetrical Gauss/Lorentz function, and then specific ratios were calculated based on the integration area.

Temperature programmed desorption

TPD analysis was carried out using apparatus equipped with gas analyzers for precise measurement of the effluent gas concentrations. Before desorption, sample of 0.5 g was initially exposed to HCl at 40 °C for 3 h and then blew with argon to get rid of the surface HCl gas residual. After purification, the sample was heated to 900 °C from room temperature at a heating rate of 10 °C/min under argon. Meanwhile, a GASMET FTIR Dx4000 instrument was employed at outlet to measure effluent HCl concentration, and outlet NO_X were monitored by KANE940 (U.K.).

Experimental apparatus and procedures

An experimental system, consisting of gas mixer, fixed bed reactor, FTIR gas analyzer and waste gas treatment unit, was designed for HCl adsorption experiments. In this system, a U-type quartz tube (inner diameter 20 mm) held in a vertical position was disposed in the water bath (40 ± 2°C) to form a fixed bed reactor. Before HCl capture tests, the pipelines were blew continuously by argon to remove possible gaseous impurities. The initial total gas flow rate was 1 L/min (600 ppm HCl with balanced N_2). HCl/N_2 stream was first injected to the pipelines before HCl adsorption experiments. Sample of 0.5 g was placed on the fixed bed reactor until effluent HCl concentration was stabilized at 600 ppm for several minutes. Then the evolution of outlet HCl was monitored and recorded. After sample reached saturation, a purge step by argon (1 L/min) was applied subsequently, followed by a TPD step.

Performance of the carbon samples

The HCl removal efficiency η in equation (1) was defined to assess the HCl retention ability for individual carbon sample. Furthermore, breakthrough time, defined as the duration when η is over 90%, is another index to evaluate the performance of adsorbents. For all materials, the effluent HCl gas concentrations were recorded, and the efficiencies can be calculated accordingly.

$$\eta = (1 - C_{outlet}/C_{intlet}) \times 100\% \quad (1)$$

where C_{inlet} and C_{outlet} respectively represent inlet and outlet HCl gas concentrations in the unit of ppm.

Results and discussions

Textural properties

The textual properties were characterized by N_2 adsorption and typical nitrogen isotherms at 77 K are given in Figure 1. As recommended by IUPAC, the hysteresis loop of type H4 may associates with specific pore structures which have been obtained with adsorbents having slit-shaped pores[26]. Table 1 lists the textural properties and atom ratios of O/C and N/C from elemental analysis. Figure 2 presents the pore size distribution of the ACF-AR. It can be found that ACF-AR has

BET surface area (S_{BET}) of 1270 m^2/g, total pore volume (V_{total}) of 0.56 cm^3/g, micropore volume (V_{micro}) of 0.35 cm^3/g and adsorption average pore size (D_{pore}) of 1.78 nm, indicating its high porosity.

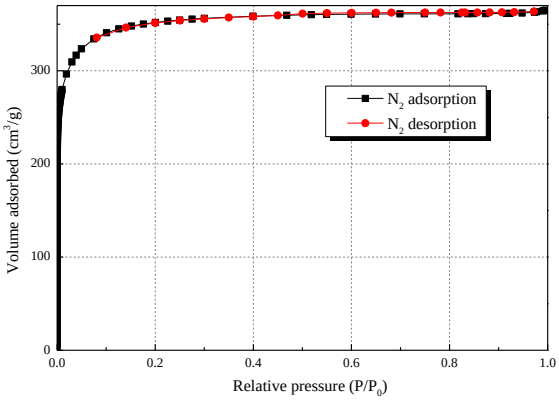

Figure 1 Typical nitrogen isotherms (ACF-AR) at 77K

Table 1 Textual properties of the viscose-based ACFs

Sample	S_{BET}	V_{total}	V_{micro}	D_{pore}	Atom ratio	
	m^2/g	cm^3/g	cm^3/g	nm	O/C	N/C
ACF-AR	1270	0.56	0.35	1.78	0.09	0.019
ACF-1	1263	0.55	0.36	1.70	0.07	0.024
ACF-2	1248	0.55	0.35	1.78	0.13	0.012
ACF-3	1132	0.51	0.34	1.78	0.11	0.036
ACF-4	1098	0.49	0.30	1.77	0.09	0.038

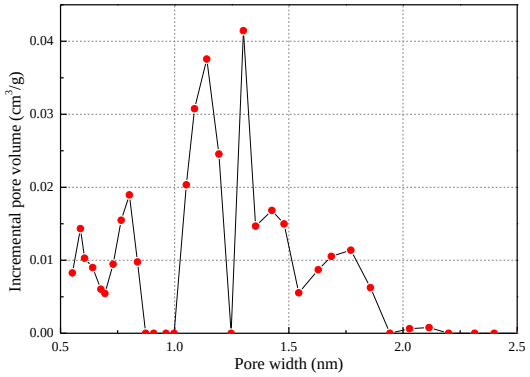

Figure 2 Pore size distribution of ACF-AR

For sample ACF-1, both S_{BET} and the average pore width were diminished while micropore volume almost keep the same. According to Table 1, the average pore size decreased because macropore can be shrunk by thermal treatment[27]. In the case of ACF-2, the decrease of S_{BET} can be attributed to the slight decline of pore volume. For ACF-3 and ACF-4, S_{BET} were even reduced by over 10 % due to the decline of mesopore and/or macropore volume. Micropore structure in ACF-4 can be damaged by the pore blocking from surface oxygen groups into some micropores [28]. In addition, S_{BET} and the total pore volume of ACF-4 declined much more than those of ACF-3 while the average pore size of ACF-4 keep the same as ACF-3, further indicating that $Cu(NO_3)_2$ treatment did block the macropore instead of micropore. SEM images of ACF-AR and ACF-4 are presented in Figure 3 to study the changes of surface morphology. It can be observed that carbon surface was uniformly modified after $Cu(NO_3)_2$ modification, leading to the decline of S_{BET} and the total pore volume.

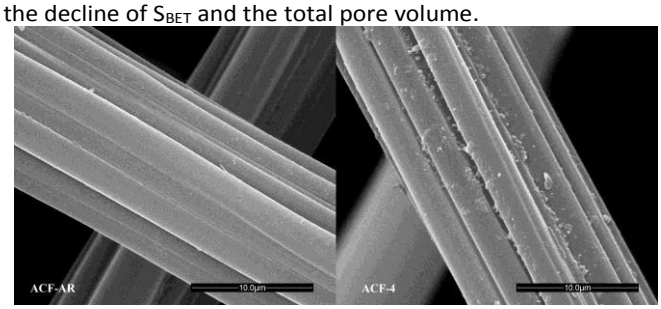

Figure 3 SEM images of ACF-AR and ACF-4

Surface chemistry

Specific ratios of surface oxygen groups from XPS C1s spectra were provided in Figure 4. The spectra consist of carbide carbon (C-C, binding energy (BE) 283.1 ± 0.2 eV, full width half maximum (FWHM) 0.8 ± 0.3 eV), alkene carbon (C-C, BE 283.8 ± 0.1 eV, FWHM 0.7 ± 0.2 eV), graphite carbon (C-C, BE 284.3 ± 0.2 eV, full FWHM 1.4 ± 0.2 eV), carbon species in alcohol, ether functional groups (C-O, BE 285.0 ± 0.5 eV, FWHM 2.0 ± 0.3 eV), carbonyl functional groups (C=O, BE 286.5 ± 0.4 eV, FWHM 2.3 ± 0.2 eV), carboxyl and/or ester functional groups (COO, BE 288.5 ± 0.4 eV, FWHM 2.1 ± 0.5 eV), and graphitic shake-up peak from π-π transitions in aromatic rings (π-π, BE 290.4 ± 0.3 eV, FWHM 2.6 ± 0.3 eV) [29]. The amounts of C-C, C-O, C=O, COO and π-π respectively account for 18.86%, 28.51%, 24.24%, 17.28%, and 11.11% over the surface of ACF-AR.

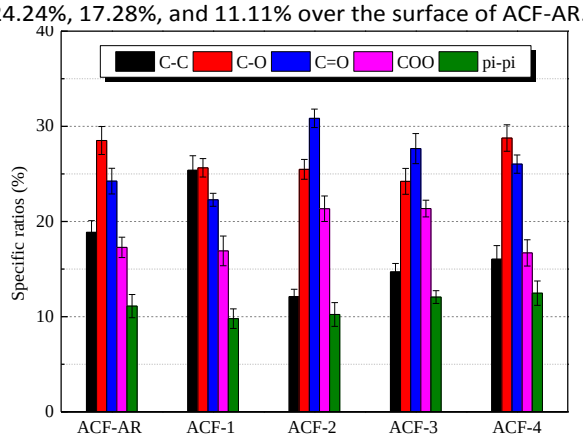

Figure 4 Specific ratios of C1s surface groups for the ACFs

In the case of ACF-1, the specific ratio of C-C increased significantly while the amount of C-O and C=O decreased slightly. Thermal treatment reduced the amount of C-O and C=O, and reformed to C-C by inducing secondary reactions at high temperature[27, 30, 31]. For sample ACF-2 and ACF-3, the increase of C=O and COO, as well as the decrease of C-C can be owned to severe oxidation by H_2O_2 and nitric acid[27, 29, 32]. As for ACF-4, the amount of C=O was slightly increased while the

contents of other oxygen species kept the same as ACF-AR, indicating that $Cu(NO_3)_2$ has very limited impact on surface oxygen-containing groups. Moreover, the slight change in surface oxygen groups may associate with the change of total acidity from $Cu(NO_3)_2$ treatment.

Figure 5 displays the specific ratios of nitrogen groups over the ACFs surface before and after modifications, and the ratios of surface nitrogen groups before and after HCl adsorption experiments were simultaneously presented in Figure 6. Data of ACF-1 and ACF-2 are not given because no obvious change in nitrogen groups were detected after treatments. For ACF-3 and ACF-4 in Figure 5, the amounts of pyrrole, pyridine and quaternary nitrogen sharply dropped, while the specific ratios of N-O kept the same. As shown in the histogram, new nitrogen species, i.e. $-NO_2$ and $-NO_3$, were newly formed after modification. Overall, nitrogen groups were significantly modified since N treatment could fix nitrogen functional groups on external and/or internal surface [29]. From Figure 6, after HCl uptake the amounts of $-NO_2$ and $-NO_3$ respectively experienced reductions of 73%, 14% for ACF-3, and 61%, 36% for ACF-4, while the specific ratios of other nitrogen groups were all increased. It is notable that the content of $–NO_2$ decreased much more than that of $–NO_3$ after capture HCl.

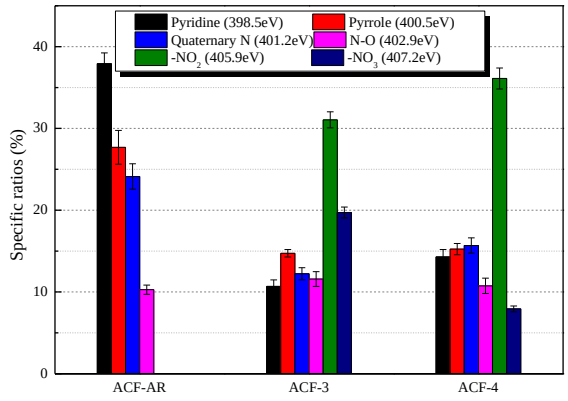

Figure 5 Specific ratios of N1s surface groups for the ACFs

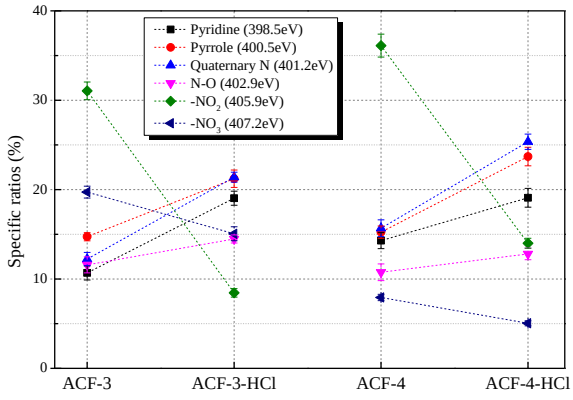

Figure 6 Specific ratios of surface nitrogen groups for the ACFs before (ACF-3, ACF-4) and after (ACF-3-HCl, ACF-4-HCl) HCl adsorption

Figure 7 shows XPS Cl2p spectra of the ACF-3 and ACF-4 with HCl adsorption. The binding energies around 201.1 eV in the spectra can be attributed to the chlorine atoms chemically boned onto the ACFs.

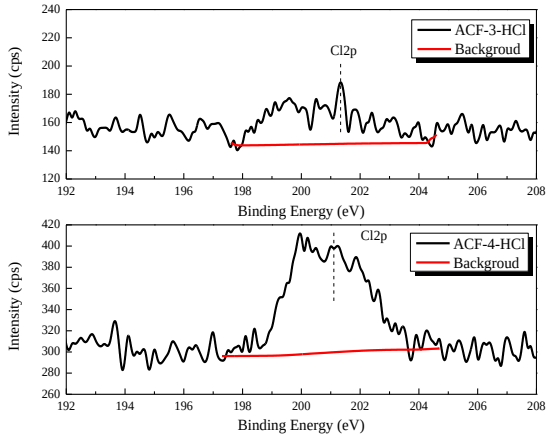

Figure 7 XPS Cl2p spectra of ACF-3-HCl and ACF-4-HCl

Hydrogen chloride removal

Figure 8 shows the evolution profiles of HCl removal efficiency over time. In particular, the time-efficiency curves also highlight the breakthrough time for different samples. The ACFs display very similar efficiency curves except for th difference in breakthrough time. In the initial stage, adsorption into the micropores led to a sharp increase in the removal efficiency. After then, active sites over porous carbon were gradually occupied by HCl molecules. With the proceeding of adsorption, the HCl removal efficiency decreased to zero, indicating the total breakthrough of the ACFs.

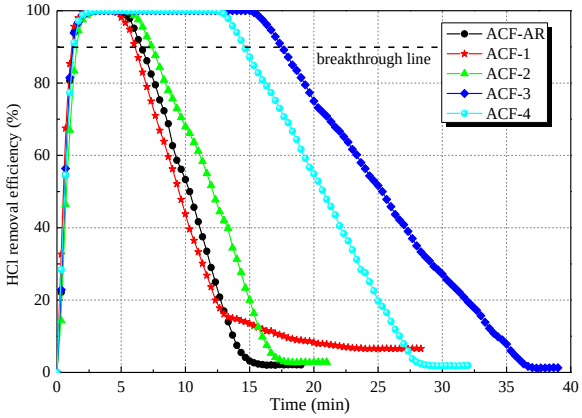

Figure 8 The removal efficiency of HCl gas for the ACFs

In the case of ACF-1, breakthrough time was slightly shortened after thermal treatment at 900 °C, as thermal treatment can influence not only the carbon textural properties but also the distribution of surface oxygen groups[27] and thus reduce the HCl retention ability over the ACFs surface. Interestingly, ACF-1 exhibited different adsorption behavior from other ACFs whe the efficiency is below 10%, however, rare research w s carried out to investigate HCl adsorption over the ACFs surface and detailed mechanism still need further efforts, thou n adsorption behaviors of other acidic gases (i.e. SO_2, NO and

H_2S) over thermal treated ACFs have been investigated by many scholars[3, 8, 13, 33].

ACF-2 showed an extremely similar profile as ACF-AR except for the extended period of complete breakthrough. Changes in surface chemistry showed that the amounts of C-C and C-O were reduced and relative ratios of C=O and COO were increased after H_2O_2 treatment. Perhaps oxygen groups, such as C=O and COO, should take responsibility for the enhancement of retention ability over the carbon surface, since they can significantly affect the transport of HCl molecules adsorbed into microspores[18, 34, 35].

The breakthrough time of ACF-3 and ACF-4 were extended from 360 to 1050 and 900 s respectively. Unfortunately, changes in the textural properties (in Table 1) could not support the enhancement of HCl removal since both ACF-3 and ACF-4 have a lower specific surface area than that of ACF-2. XPS analysis in Figure 4 revealed that the ratios of surface oxygen groups, in particular the C=O and COO, were increased after modification, nevertheless, the slight increase of surface oxygen groups may enhance HCl removal but could not precisely interpret why removal efficiencies of ACF-3 and ACF-4 were improved so much. In other words, there must be other factors conducive to HCl adsorption. The newly formed nitrogen groups could be the most probable reason for the improvement of removal efficiency, according to Figure 5. Furthermore, sharp decrease of $–NO_2$ and $–NO_3$ were observed in Figure 6 after HCl adsorption, suggesting the significant promotion effect of $–NO_2$ and $–NO_3$ over the removal of HCl. Notably, adsorption processes consumed much more $–NO_2$ than $–NO_3$, indicating the more important role of $–NO_2$ than $–NO_3$ during adsorption. This interesting phenomenon can be explained by following assumptions. $–NO_2$ group can be substituted by chlorine atoms in adsorbed HCl ($HCl_{(ads)}$) molecules and generated chlorides and adsorbed HNO_2 ($HNO_{2\ (ads)}$). Meanwhile, $HNO_{2\ (ads)}$ can be oxidized to HNO_3. Both HNO_2 and HNO_3 are not stable and thus easy to be decomposed to NO and/or NO_2. $-NO_2$ was consumed much more than $–NO_3$ due to the lower stability of $-NO_2$ groups. Possible reaction pathways are presented in Figure 9.

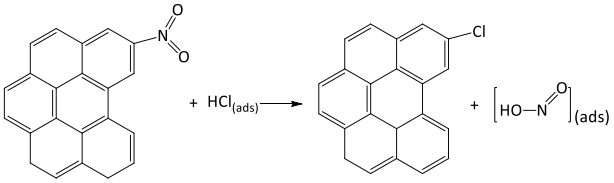

Figure 9 Possible HCl adsorption products and the mechanisms that are proposed for the consumption of nitrogen groups.

Temperature programmed desorption

TPD analysis is effective to investigate HCl gas adsorption over the ACFs surface. Figure 10 respectively shows the TPD profiles for the ACFs before (ACF-3, ACF-4) and after (ACF-3-HCl, ACF-4-HCl) HCl adsorption.

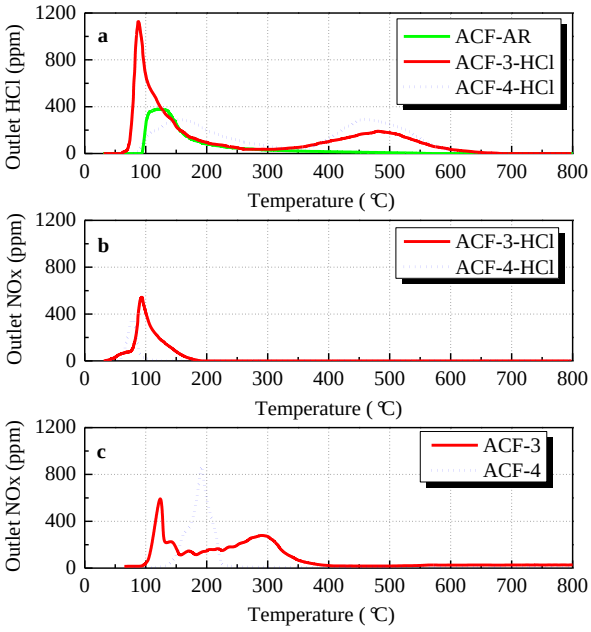

Figure 10 TPD analysis for the ACFs before (ACF-3, ACF-4) and after (ACF-3-HCl, ACF-4-HCl) HCl adsorption

In Figure 10(a), there is only one HCl desorption peak for ACF-AR, whereas two peaks appeared for ACF-3 and ACF-4. In the initial stage (<150 °C), all materials released significant amount of HCl due to gas desorption from the carbon micropores. However, ACF-3 released much more HCl than ACF-AR while actually ACF-3 has a 10% lower specific surface area than ACF-AR. A possible explanation could be that the first desorption peak come from enhanced physical adsorption[19]. Subsequently, the outlet HCl concentration started to decline, yet an increa in outlet HCl concentration was noted again for ACF-3 and ACF-4 when temperature was over 400 °C, followed by a gradual decline to zero. Overall speaking, ACF-3 exhibited different desorption behaviors from ACF-4.

According to TPD profiles in Figure 10(b), ACF-3 desorbed much more NO_X than ACF-4 mainly since adsorbed HCl molecules could interact with $–NO_2$/ $–NO_3$ groups and generate HNO_2 and/or HNO_3 over the ACFs surface. Meanwhile, both HNO_2 and HNO_3 are unstable and thus can be decomposed into nitrogen oxides, i.e. NO and NO_2, which can be liberated in the form of NO_X at elevated temperature. Moreover, HNO_3 treatment could significantly impact the totally acidity of the ACFs surface, which favored the formation of acidic gases. Hence a considerable amount of NO_X was emitted for ACF-3 while only a small amount of NO_X was released for ACF-4 at lower temperature. However, with th proceeding of desorption, no more NO_X was detected after 200 °C probably due to the depletion of surface nitrogen species.

TPD analysis in Figure 10(c) was provided to understand th desorption behavior of ACF-3 and ACF-4 for comparison. Fo ACF-3, $-NO_2$/$-NO_3$ over the carbon surface started decompose at 100 °C and released significant amount of NO

until 400 °C, while in the case of ACF-4, NO_X was detected in the effluent gas until 150 °C. Moreover, the temperature area of ACF-4 is much narrower than that of ACF-3. These interesting phenomena can be explained by the thermal decomposition of -NO_2 and/or -NO_3. -NO_2 can be gently decomposed at low temperature while -NO_3 can be quickly decomposed at high temperatures[36].

Interestingly, after 200 °C no more NO_X was desorbed for both ACF-3-HCl and ACF-4-HCl, indicating -NO_2/-NO_3 groups over the ACFs surface were mostly consumed in HCl adsorption process. However, the reactions among HCl molecules, -NO_2/-NO_3 groups, copper ion and carbon surface requires further effort since they could interacted with each other over the ACFs surface to form complex compounds[37]. Fortunately, no matter what happened over the ACFs surface, nitrogen groups, especially the –NO_2 and –NO_3, exhibited significant promotion on the removal of HCl gas.

Conclusions

In this paper, both physical and chemical methods, covering a wide range of porous texture and surface chemistry, were employed to treat viscose-based ACFs, and extensive information was obtained about the roles of oxygen and nitrogen groups on HCl removal. Thermal treatment could accelerate the decomposition of oxygen groups and decrease the HCl retention ability, while H_2O_2 enriches surface oxygen groups and can enhance HCl adsorption. Moreover, O-containing nitrogen groups can be introduced onto the ACFs surface using nitric acid and copper nitrate treatments, and significantly improved the performance of ACFs on HCl adsorption. The current work indicates that both oxygen and nitrogen groups over the ACFs surface could promote the removal of HCl gas. Surprisingly, -NO_2/-NO_3 containing ACFs could even extend the breakthrough time to almost triple that of untreated ACFs. In addition, adsorption processes consumed much more -NO_2 than -NO_3 group, indicating the significant role of -NO_2 group in removing HCl molecules. Therefore, surface nitrogen species, i.e. -NO_2 and -NO_3 groups, can be effective modification methods to enhance the removal of HCl over the carbon surface.

Acknowledgements

This work is supported by the National Science Foundation of China (Grant Nos. 50976041, 51276074) and Innovation Research Foundation of Huazhong University of Science and Technology (2014NY008).

Notes and references

1. F. Caiazzo, A. Ashok, I. A. Waitz, S. H. L. Yim and S. R. H. Barrett, *Atmospheric Environment*, 2013, **79**, 198-208.
2. D. Vallero, in *Fundamentals of Air Pollution (Fifth Edition)*, ed. D. Vallero, Academic Press, Boston, 2014, DOI: http://dx.doi.org/10.1016/B978-0-12-401733-7.00031-1, pp. 881-925.
3. C. Yao, Z. Jiayong and W. Zuwu, *Plasma Science and Technology*, 2013, **15**, 1047.
4. Z. M. Sun, Y. C. Yu, S. Y. Pang and D. Y. Du, *Applied Surface Science*, 2013, **284**, 100-106.
5. S. Y. Lee and S. J. Park, *Journal of Colloid and Interface Science*, 2013, **389**, 230-235.
6. R. C. Bansal and M. Goyal, *Activated carbon adsorption*, CRC press, 2010.
7. B.X. Shen, Y.C. Zhou, Z.L. Shi and T.T. Yang, *Journal of Fuel Chemistry and Technology*, 2008, **36**, 376-380.
8. J. Guo, Y. Luo, A. C. Lua, R. A. Chi, Y. L. Chen, X. T. Bao and S. X. Xiang, *Carbon*, 2007, **45**, 330-336.
9. S.J. Park and B.J. Kim, *Journal of Colloid and Interface Science*, 2005, **282**, 124-127.
10. H. C. Zeng, F. Jin and J. Guo, *Fuel*, 2004, **83**, 143-146.
11. H.H. Tseng, M.Y. Wey, Y.S. Liang and K.H. Chen, *Carbon*, 2003, **41**, 1079-1085.
12. W. M. Qiao, Y. Korai, I. Mochida, Y. Hori and T. Maeda, *Carbon*, 2002, **40**, 351-358.
13. I. Mochida, Y. Korai, M. Shirahama, S. Kawano, T. Hada, Y. Seo, M. Yoshikawa and A. Yasutake, *Carbon*, 2000, **38**, 227-239.
14. C. L. Mangun, K. R. Benak, M. A. Daley and J. Economy, *Chemistry of Materials*, 1999, **11**, 3476-3483.
15. M. Suzuki, *Carbon*, 1994, **32**, 577-586.
16. I. Mochida, H. Toshima, Y. Korai and T. Naito, *Journal of Materials Science*, 1988, **23**, 678-686.
17. I. Mochida, S. H. Yoon, N. Takano, F. Fortin, Y. Korai and K. Yokogawa, *Carbon*, 1996, **34**, 941-956.
18. S. J. Park and B. J. Kim, *Journal of Colloid and Interface Science*, 2004, **275**, 590-595.
19. C. L. Mangun, K. R. Benak, J. Economy and K. L. Foster, *Carbon*, 2001, **39**, 1809-1820.
20. Y. Y. Guo, Y. R. Li, T. Y. Zhu and M. Ye, *Fuel*, 2015, **143**, 536-542.
21. S. Adapa, V. Gaur and N. Verma, *Chemical Engineering Journal*, 2006, **116**, 25-37.
22. S. Brunauer, P. H. Emmett and E. Teller, *Journal of the American Chemical Society*, 1938, **60**, 309-319.
23. B. C. Lippens and J. H. de Boer, *Journal of Catalysis*, 1965, **4**, 319-323.
24. R. S. Mikhail, S. Brunauer and E. E. Bodor, *Journal of Colloid and Interface Science*, 1968, **26**, 45-53.
25. M. El-Merraoui, M. Aoshima and K. Kaneko, *Langmuir*, 2000, **16**, 4300-4304.
26. H. H. Tseng, M. Y. Wey and C. H. Fu, *Carbon*, 2003, **41**, 139-149.
27. G. De la Puente, J. J. Pis, J. A. Menendez and P. Grange, *Journal of Analytical and Applied Pyrolysis*, 1997, **43**, 125-138.
28. J. W. Shim, S. J. Park and S. K. Ryu, *Carbon*, 2001, **39**, 1635-1642.
29. C. Moreno Castilla, M. Lopez Ramon and F. Carrasco Marın, *Carbon*, 2000, **38**, 1995-2001.
30. Y. Otake and R. G. Jenkins, *Carbon*, 1993, **31**, 109-121.
31. P. J. Hall and J. M. Calo, *Energy and Fuels*, 1989, **3**, 370-376.
32. J. Cheng, J. H. Zhou, J. Z. Liu, Z. J. Zhou, Z. Y. Huang, X. Y. Cao, X. Zhao and K. F. Cen, *Progress in Energy and Combustion Science*, 2003, **29**, 381-405.
33. Z.S. Liu, *Waste Management*, 2008, **28**, 2329-2335.
34. D. D. Duong, ed., *Adsorption Analysis: Equilibria and Kinetics*, Imperial College Press, London, 1998.
35. F. L. Y. Lam and X. Hu, *Chemical Engineering Science*, 2003, **58**, 687-695.
36. J. Ghose and A. Kanungo, *Journal of Thermal Analysis and Calorimetry*, 1981, **20**, 459-462.

37. S. Biniak, M. Pakula, G. Szymanski and A. Swiatkowski, *Langmuir*, 1999, **15**, 6117-6122.